https://doi.org/10.5194/essd-2021-452
Preprint. Discussion started: 31 March 2022

Earth System Science Data
Open Access Discussions

Title: Vegetation photosynthetic phenology metrics in northern terrestrial ecosystems: a dataset derived from a gross primary productivity product based on solar-induced chlorophyll fluorescence

Jing Fang[1,2], Xing Li[3], Jingfeng Xiao[4], Xiaodong Yan[5], Bolun Li[3], Feng Liu[1,2]*

1 CAS Key Laboratory of Aquatic Botany and Watershed Ecology, Wuhan Botanical Garden, Chinese Academy of Sciences, Wuhan 430074, China

2 Center of Plant Ecology, Core Botanical Gardens, Chinese Academy of Sciences, Wuhan, 430074, China

3 Research Institute of Agriculture and Life Sciences, Seoul National University, Seoul, South Korea

4 Earth Systems Research Center, Institute for the Study of Earth, Oceans, and Space, University of New Hampshire, Durham, NH, USA

5 State Key Laboratory of Earth Surface Processes and Resource Ecology, Faculty of Geographical Science, Beijing Normal University, Beijing 100875, China

https://doi.org/10.5194/essd-2021-452
Preprint. Discussion started: 31 March 2022

Corresponding author: Feng Liu (liufeng@wbgcas.cn)

Postal address of the corresponding author: Chinese Academy of Sciences, Wuhan 430074, China

Abstract

Vegetation phenology can profoundly modulate the climate-biosphere interactions and thus plays a key role in regulating the terrestrial carbon cycle and the climate. However, most previous phenology studies are based on the traditional vegetation indices, which are inadequate to characterize the seasonal activity of photosynthesis. Here, we generated an annual vegetation photosynthetic phenology dataset with a spatial resolution of 0.05 degree from 2001 to 2020, using the latest gross primary productivity product based on solar-induced chlorophyll fluorescence (GOSIF-GPP). We combined smoothing splines with multiple change-point detection to retrieve the phenology metrics: start of the growing season (SOS), end of the growing season (EOS), and length of growing season (LOS) for terrestrial ecosystems in the Northern Hemisphere. We found that the derived phenology metrics agreed better with in situ observations

https://doi.org/10.5194/essd-2021-452
Preprint. Discussion started: 31 March 2022

from the flux tower sites than vegetation indices and MODIS-GPP. Our phenology metrics captured the spatial-temporal patterns of the single and double growing season in the Northern Hemisphere. The double season was mainly from the cropland rotation and ecosystems having two different phenological cycles. In addition, we observed a trend toward advanced SOS in about 62.98% of the land area, with a mean rate of 0.14±0.01 days year^{-1}, a trend toward delayed EOS in about 61.87% of the area, with a mean rate of 0.19±0.16 days year^{-1}, and a trend toward extended LOS in about 70.52% of the area, with a mean rate of 0.33±0.17 days year^{-1}. Our phenology product can be used for validating and developing phenology models or carbon cycle models, for evaluating satellite remote sensing phenology, and for monitoring climate change impacts on terrestrial ecosystems. The data are available at https://doi.org/10.6084/m9.figshare.17195009.v2 (Fang et al. 2021).

1. Introduction

Vegetation phenology, the cycle sequence of plant vital activities, is a highly sensitive indicator of the climate impacts on terrestrial ecosystems (Richardson et al. 2013, Piao

https://doi.org/10.5194/essd-2021-452
Preprint. Discussion started: 31 March 2022

et al. 2019, Wang et al. 2019, Keenan et al. 2020). Most phenology studies focus on the structural changes of plants, such as using the growth process of leaf represented by the greenness indicators (Seyednasrollah et al. 2021, Yang and Noormets 2021). However, recent studies found that the methods based on vegetation greenness have limited ability to capture the photosynthesis changes in some vegetation types (e.g. evergreen forests) since the greenness and photosynthesis are sometimes decoupled (Walther et al. 2016, Smith et al. 2018). The inaccurate estimation of phenology can lead to substantial uncertainties in the estimation of plant productivity and carbon sequestration (Richardson et al. 2012, Wu et al. 2017, Fang et al. 2020).

The plant photosynthetic cycle on the seasonal time scale is termed as 'vegetation photosynthetic phenology', which represents the functional aspects of plant activities (Gu et al. 2009). This phenology definition is based on the photosynthesis transition dates extracted from the gross primary productivity (GPP) time series. Thus, the accuracy of extracted phenology metrics is largely dependent on the data source of GPP. Currently, the GPP can either be derived from Eddy Covariance (EC) flux towers at the ecosystem scale or from satellite remote sensing or modeling at the regional or global

https://doi.org/10.5194/essd-2021-452
Preprint. Discussion started: 31 March 2022

scale (Xiao et al. 2019). The EC technique, which is considered as the most accurate observation method (Baldocchi et al. 2001), has provided long-term GPP estimates for more than 20 years. However, these observations are limited by their spatial distribution and some key areas are still underrepresented (Xiao et al. 2019). For example, only a few EC sites provide public datasets in the tropical and high latitude regions. GPP derived from satellite remote sensing is able to investigate large–scale phenology across the globe (Sjöström et al. 2013). Greenness-related vegetation indices such as the normalized difference vegetation index (NDVI) and the enhanced vegetation index (EVI) have been widely used to estimate GPP (Wu et al. 2017, Huang et al. 2019, Dai et al. 2021). However, these indices work better for capturing the variations in chlorophyll content or vegetation coverage and are not sufficient to track the instantaneous physiological changes in vegetation photosynthesis, especially for evergreen vegetation (Joiner et al. 2014, Li and Xiao 2020). Recently, the emergence of satellite-based solar-induced chlorophyll fluorescence (SIF) has offered unprecedented opportunities for developing more accurate photosynthetic phenology data products on large scales (Joiner et al. 2011, Frankenberg et al. 2014, Li et al. 2018,

https://doi.org/10.5194/essd-2021-452
Preprint. Discussion started: 31 March 2022

Köhler et al. 2018). SIF, a signal emitted by plant chlorophyll molecules after absorbing photosynthetically active radiation (APAR), is considered to be an effective tool for diagnosing terrestrial photosynthesis and estimating GPP more accurately (Meroni et al. 2009, Verma et al. 2017, Wood et al. 2017, Li and Xiao 2020). Based on the SIF product, recent studies used the relationship between the GPP and SIF to estimate the regional or global GPP (SIF-GPP) (Li and Xiao 2019, Zhang et al. 2020). Previous studies reported that SIF-GPP can better capture the GPP dynamics in evergreen vegetation and dryland ecosystems than traditional vegetation indices (Bertani et al. 2017, Smith et al. 2018).

In addition, the retrieval of phenology in previous studies mainly used a logistic regression model to fit the time series of smoothed vegetation indices or GPP, and the predetermined thresholds or inflection points are identified as the transition dates of phenology in the fitted curve (Garrity et al. 2011, Wang et al. 2017, Yang and Noormets 2021). However, this method needs to reconstruct the original data sequence and thus results in uncertainty from the model parameterization (Klosterman et al. 2014). Furthermore, this method is usually used to capture a single growing season instead of

https://doi.org/10.5194/essd-2021-452
Preprint. Discussion started: 31 March 2022

the multiple growing seasons in a given year (Yang and Noormets 2021). Correspondingly, Richardson et al. (2018) proposed a method of smoothing spline and multiple change-point detection to retrieve the transition dates of phenology from the camera data. The strength of this method is not limited by the uncertainty of additional model parameters and can also be applied in ecosystems having multiple growing seasons. The method has been successfully used at multiple sites in North America (Richardson et al. 2018) and needs to be extended to large scales.

Here, we aim to generate a photosynthetic phenology metrics dataset based on the GPP product derived from satellite SIF data. Our data can detect multiple growing seasons, which can be used to evaluate the photosynthesis activity of vegetation from large scales. The metrics include the start state-transition dates of photosynthesis (SOS), the end state-transition dates of photosynthesis (EOS), and the duration length of photosynthesis (LOS). With this goal, we constructed a method combining smoothing filter and change-point detection to retrieve photosynthetic phenology from a recently developed SIF-based GPP product (GOSIF-GPP: 2001-2020) with a fine spatial resolution (0.05°). This method enables us to acquire multiple photosynthesis activity

https://doi.org/10.5194/essd-2021-452
Preprint. Discussion started: 31 March 2022

periods of vegetation within one year. The remainder of this paper describes the data of SIF-GPP and land cover data, the adopted method for retrieving photosynthetic phenology metrics, the results and discussion of the metrics and their uncertainties, and the conclusions.

2. Data

We used the GOSIF-GPP dataset from 2001-2020 (Li and Xiao 2019) to derive the phenology metrics on large scales in this study (http://data.globalecology.unh.edu/). GOSIF-GPP was estimated from the GOSIF dataset based on eight linear SIF-GPP relationships with 0.05° spatial and 8-day temporal resolutions (i.e., 46 GPP estimates per year for each 0.05° grid cell). The GOSIF dataset was developed by using discrete SIF soundings from the Orbiting Carbon Observatory-2 (OCO-2), remote sensing data from MODIS, and reanalysis data from MERRA-2 based on machine learning method (Li and Xiao 2019b). The GOSIF-GPP showed reasonable seasonal and spatial patterns and was highly correlated with GPP from FLUXNET (Li and Xiao 2019). Here, we

https://doi.org/10.5194/essd-2021-452
Preprint. Discussion started: 31 March 2022

identified the vegetation type of each grid cell according to the MODIS Land Cover Type Product Version 6 (MCD12C1: https://lpdaac.usgs.gov/products/mcd12q1v006/) (**Fig. S1**, 0.05° spatial resolution). The current study used six broad vegetation types (i.e. **forests**: evergreen needleleaf forests, evergreen broadleaf forests, deciduous needleleaf forests, deciduous broadleaf forests, and mixed forests; **shrublands**: closed canopy shrublands and open shrublands; **savannas**: savannas and woody savannas; **grasslands**; **wetlands**; **croplands**) in the Northern Hemisphere. For the sake of reducing noise generated by non-vegetation signals, we excluded the area covered with bare soil and sparse vegetation (i.e., maximum GPP lower than 2.0 g C m^{-2} day^{-1}) (Liu et al. 2016). Since the seasonal variation of vegetation photosynthesis in the tropical region is relatively small (Piao et al. 2019), we focused on the area above 30° N latitude. The final dataset is provided at each 0.05° grid for 20 years in the six terrestrial ecosystems of the Northern Hemisphere.

To evaluate phenology estimates based on GOSIF-GPP, we used the daily GPP data from EC flux towers across the Northern Hemisphere based on the FLUXNET2015 Dataset (https://fluxnet.org/data/fluxnet2015-dataset/) (Pastorello et al.

https://doi.org/10.5194/essd-2021-452
Preprint. Discussion started: 31 March 2022

Open Access Earth System Science Data Discussions

2020). We retained the EC flux sites that were relatively homogeneous because the footprint of 0.05º GOSIF product and EC tower may not exactly match (Li and Xiao 2019). We selected the flux sites having available GPP data for more than one year. The selected flux tower GPP dataset includes 49 sites with 389 site-year data (the detailed information of these flux sites can be found in **Table S1**). As a comparison, we also compared the performance of GOSIF-GPP based phenology metrics with those based on the vegetation indices and GPP products from the MODIS datasets. For each site, we extracted and calculated three vegetation indices from the Nadir Bidirectional Reflectance Distribution Function (BRDF)-Adjusted Reflectance dataset MCD43A4 (produced daily and 500 m resolution) including the NDVI, the EVI, the near-infrared reflectance of vegetation (NIRv) (Badgley et al. 2017), and the 8-day, 500-m MODIS GPP data (MOD17A2) (Zhao et al. 2005) from 2001 to 2014.

3. Method

3.1 Photosynthetic phenology metrics

https://doi.org/10.5194/essd-2021-452
Preprint. Discussion started: 31 March 2022

Open Access Earth System Science Data Discussions

The phenology metrics in this study include SOS, EOS, and LOS. Unlike the traditional phenological events from the structural changes of leaf or flower, the photosynthetic phenology is defined as the start (i.e. SOS) and end (i.e. EOS) state-transition dates of the photosynthesis cycles. These transition dates are used as the phenology metrics. One full cycle generally has five distinctive stages, including (1) photosynthesis dormancy period, a season before the growing season; (2) photosynthesis development period, a GPP rising stage; (3) photosynthesis peak period, a peak stage of GPP; (4) photosynthesis recession period, a GPP falling stage; and (5) photosynthesis dormancy period, the photosynthetically inactive stage after the growing season. Most previous studies used the sigmoid-based methods (e.g., double-logistic model) to extract the phenology, but these methods are limited to the single cycle (Yang and Noormets 2021). Because some regions or ecosystems had multiple cycles in one year, we used the smoothing splines and change points to identify the transition dates of photosynthesis. In this study, all transition dates were extracted from the daily GPP sequence of each grid cell. Thus, we interpolated the 8-day GOSIF-GPP data to the daily scale using cubic spline interpolation before the extraction.

https://doi.org/10.5194/essd-2021-452
Preprint. Discussion started: 31 March 2022

We constructed an automatic method to retrieve transition dates (i.e. SOS and EOS) of photosynthetic phenology using GPP data. The algorithm of this method is outlined in the flowchart in **Fig. 1**. The important basis for acquiring phenological events was the data reconstruction using smoothing methods to minimize the impact of abnormal values (Li et al. 2019). We applied the iterative procedure to conduct the smoothing process (**Fig. 1**): (1) Smoothing the GPP time series by the Savitzky-Golay filter, which can reflect the change characteristics of the original data sequence; (2) Calculating the ratio of the daily GPP value to the smooth value; (3) Identifying outliers in these ratios by using the Grubbs test; (4) Using the smooth value instead of the daily GPP value when the ratios were larger than one standard deviation below the mean ratio; (5) Applying the iterative procedure up to 20 times or until no outliers were detected from one iteration to the next. This procedure can largely keep the raw seasonal pattern of photosynthesis and avoid the uncertainty of parameter estimation by reconstructing the data time series by estimating parameters in the double logistic model.

The potential change points in the final smoothing splines were identified with the Pruned Exact Linear Time (PELT) method. This method can accurately detect the

https://doi.org/10.5194/essd-2021-452
Preprint. Discussion started: 31 March 2022

significant change points in the data time series and does not need to preset the number of change points. The PELT was first applied by Killick et al. (2012), and they described in detail on how to find the change points in time series. For each photosynthesis cycle, we followed Richardson et al. (2018) to set the penalty factor and the minimum segment length of PELT as 0.5 and 14-days, respectively. We calculated the mean GPP value of the adjacent change points as the potential peak and bottom baseline in one full cycle. According to the time series of mean GPP value, we used the difference method to detect the bottoms and peaks (i.e., minimum and maximum value in each cycle). The adjacent bottoms and one peak were formed as a full cycle, and the value of these points was considered as the baselines. Some GOSIF-GPP data affected by the weak vegetation SIF signals could have unreliable cycles, and these cycles that had peaks less than 0.25 of the maximum peak were excluded in the current study.

Here, the SOS and EOS dates of each cycle were determined by amplitude thresholds. The amplitude was equal to the peak minus the bottom. Although the “true” onset of photosynthesis may correspond most closely to the 10% amplitude threshold (Wu et al. 2017), the most tightly-constrained transition dates tended to occur in the

https://doi.org/10.5194/essd-2021-452
Preprint. Discussion started: 31 March 2022

later dates of the GPP rising stage and the earlier dates of the GPP falling stage (Richardson et al. 2018). Thus, we followed Richardson et al. (2018) to provide the SOS and EOS dates by using three amplitude thresholds: 10%, 25%, and 50%. The SOS and EOS were determined when the GPP smoothing splines reached the value of amplitude thresholds, and the LOS was defined as EOS minus SOS:

$$SOS_i = t, if\ GPP_S(t) = (Peak - Bottom_1) \times threshold_i \qquad (1)$$

$$EOS_i = t, if\ GPP_S(t) = (Peak - Bottom_2) \times threshold_i \qquad (2)$$

$$LOS_i = EOS_i - SOS_i \qquad (3)$$

where i is the threshold (10%, 25%, and 50%); t is the day of the year (DOY); GPP_S is the daily value of the smoothing splines; $Bottom_1$ is the baseline for dormancy season before the growing season; $Bottom_2$ is the baseline for dormancy season after growing season. Note that we retrieved the phenology of vegetation indices (i.e. daily data) and MODIS-GPP (i.e. interpolating the 8-day data to the daily scale) by using the same method.

3.2 Uncertainty estimation

https://doi.org/10.5194/essd-2021-452
Preprint. Discussion started: 31 March 2022

The uncertainties in the estimates of phenology metrics mainly arise from the gridded SIF-based GPP estimates, such as using the limited explanatory variables to acquire the gridded SIF estimates (i.e., GOSIF) and the relationship between the SIF and GPP. In this study, we did not assess the quality of the underlying SIF and GPP data, which was previously evaluated (Li and Xiao 2019); instead we used the Monte Carlo Bootstrapping method (Efron 1992) to estimate the related uncertainties. Bootstrapping provides valuable information about uncertainties without making assumptions about the underlying data distributions (Elmore et al. 2012). For each year of the individual grid cell, we used bootstrapping to replace the transition dates with 100 times random uniform sampling (Yang and Noormets 2021). The 5th and 95th percentiles of the 100 bootstrapped data were considered as the confidence interval of the mean estimated from the original transition dates.

4. Results and discussion

4.1 Comparison with phenology derived from vegetation indices, MODIS-GPP,

https://doi.org/10.5194/essd-2021-452
Preprint. Discussion started: 31 March 2022

and EC tower data

We used the photosynthetic phenology metrics extracted from the daily GPP of the flux towers to examine the corresponding metrics extracted from the GOSIF-GPP product. We also use the same method to retrieve phenology from the NDVI, EVI, NIR$_V$, and MODIS GPP for the EC tower sites. According to the different thresholds, the metrics were divided in to nine groups (SOS$_{10\%}$, SOS$_{25\%}$, SOS$_{50\%}$: SOS with 10%, 25%, and 50% amplitude threshold; EOS$_{10\%}$, EOS$_{25\%}$, EOS$_{50\%}$: EOS with 10%, 25%, and 50% amplitude threshold; EOS$_{10\%}$, EOS$_{25\%}$, EOS$_{50\%}$: EOS with 10%, 25%, and 50% amplitude threshold) (**Fig. 2** and **Table 1**). Overall, the phenology metrics of GOSIF-GPP showed the highest correlations with the phenology metrics of EC tower GPP, while the phenology of NDVI showed the lowest correlations. For each metric, (1) SOS, the correlation coefficient (*R*) between the 10%, 25%, and 50% SOS of EC tower GPP and other data were (i.e. from high to low): GOSIF-GPP (0.78-0.80), MODIS-GPP (0.65-0.67), NIR$_V$ (0.47-0.60), EVI (0.40-0.57), and NDVI (0.14-0.39); the root mean square error (*RMSE*) were (i.e. from low to high): GOSIF-GPP (14.99-18.03 days), MODIS-GPP (18.83-22.98 days), NIR$_V$ (21.74-29.86 days), EVI (24.97-36.97 days),

https://doi.org/10.5194/essd-2021-452
Preprint. Discussion started: 31 March 2022

and NDVI (26.20-26.91 days). (2) EOS, the highest *R* between 10%, 25%, and 50% EOS of EC tower GPP and other data was GOSIF-GPP (0.63-0.73) and the lowest *R* was NDVI (0.42-0.56). (3) LOS, the highest *R* between 10%, 25%, and 50% EOS of EC tower GPP and other data was GOSIF-GPP (0.65-0.76) and the lowest *R* was NDVI (0.28-0.40). The comparisons indicated that GOSIF-GPP showed consistently better performance than the vegetation indices (i.e., NDVI, EVI, and NIRv) for different phenology metrics and different thresholds. MODIS-GPP had larger deviations compared to GOSIF-GPP, which highlights the need for the improvement on light use efficient models. NIRv, the product of near-infrared reflectance and NDVI (Badgley et al. 2017), was slightly better to capture the phenology metrics of tower GPP than EVI and NDVI. The results agreed with previous studies which showed a stronger ability of SIF in responding to the environmental conditions such as water and heat stresses, and thus in better capturing the seasonal and interannual photosynthetic activity (Walther et al. 2016; Smith et al. 2018; Li et al. 2018).

The derived phenology of GOSIF-GPP and EC tower GPP showed a close correspondence across the 389 site-years. The best performance of the different

https://doi.org/10.5194/essd-2021-452
Preprint. Discussion started: 31 March 2022

thresholds in SOS, EOS, and LOS was 25% (R=0.80, 0.73, and 0.76; RMSE=15.83, 21.89, and 29.14 days, respectively), and the threshold of 10% had relatively low performance in SOS and EOS (R=0.79 and 0.63; RMSE=18.03 and 23.55 days, respectively) and 50% had relatively low performance in LOS (R=0.65; RMSE=27.89 days). Our results showed that our method better captured the SOS than the EOS, which was consistent with previous studies that uncertainty occurred in satellite-based EOS estimations, especially for the evergreen vegetation such as tropical and boreal evergreen forests (Liu et al. 2016, Piao et al. 2019). In addition, more tower sites need to be considered in further studies so that the photosynthesis phenology metrics from the SIF product can be better evaluated.

4.2 Number of growing seasons

We used the method to retrieve the multiple growing seasons in the Northern Hemisphere. **Fig. 3** showed the spatial distribution of the number of growing seasons. Most regions in the Northern Hemisphere had a single growing season, while part of the cropland had a double growing season in a given year. The North China Plain (the

https://doi.org/10.5194/essd-2021-452
Preprint. Discussion started: 31 March 2022

red part in the top right of **Fig. 3**) had the most areas with the double growing season because the wheat-maize rotation was the most important cropping system in this plain (Zhao et al. 2006). This artificial crop rotation pattern brought two photosynthesis cycles: wheat grows in winter and spring, and maize grows in summer and autumn. In addition to croplands, a small proportion of the grid cells also had double growing seasons, such as some areas in California. Turner et al. (2020) reported that the double growing season in California was due to two overlapping ecosystems in one grid, whereas they were out of phase with each other: grasslands showed a peak of the growing season in April and forests peak in June. The phenology retrieval of such mixed ecosystems is still challenging and requires further exploration (Piao et al. 2019).

4.3 Spatial patterns of photosynthetic phenology metrics

Here, we showed the spatial distribution of the first growing season in **Fig. 4**. Overall, phenology metrics (SOS, EOS, and LOS) in terrestrial ecosystems of the Northern Hemisphere exhibited a spatially explicit pattern from the high latitudes to the low latitudes. Limited by low temperature, the areas around the Arctic Circle had the latest

https://doi.org/10.5194/essd-2021-452
Preprint. Discussion started: 31 March 2022

SOS (DOY>140), the earliest EOS (DOY<220), and the shortest LOS (days<120). LOS gradually increased as the climate conditions became more suitable for photosynthesis and then reached the longest in the subtropics. For different thresholds, the mean difference of SOS, EOS, and LOS between 10% and 50% was 30 days, 40 days, and 70 days, respectively. For different ecosystems (**Table 2**), grasslands showed the earliest SOS and EOS among all biomes; forests and savannas had the latest SOS; croplands and forests exhibited the latest EOS and the longest LOS, while shrublands and grasslands had the shortest LOS.

Fig. 5 showed the spatial distribution of the second growing season. We found that the second 10% SOS in North China Plain was in the end of May (DOY=150) and the second 10% EOS was in the middle of September (DOY=280). This was consistent with the emergence and dormancy of maize (i.e. the second growing season). The wheat would seed after the maize was harvested and the greenness of wheat was in the early March of the next year, which was the start time of the first growing season (Tang et al. 2020). In California, the second 10% SOS of some areas was in the early June (DOY=160) and 10% EOS was in the middle of September (DOY=280); the second

https://doi.org/10.5194/essd-2021-452
Preprint. Discussion started: 31 March 2022

10% SOS of other areas was in the late September (DOY=250) and 10% EOS was in the late November (DOY=330). These results were from the two different mixed grids, one included the evergreen forests and grasslands, another included the croplands and grasslands. Turner et al. (2020) found that the growth of grasses provides the first growing season for these grids. As the grids included evergreen forests entered summer, the increase of the available water in the soil resulted in the growth of evergreen woody plants, prompting these grids to enter the second growing season. Other ecosystems were gradually entered the dormant stage in fall, but the crops still maintained photosynthesis, making the grids containing croplands show the second growing season.

4.4 Uncertainties of photosynthetic phenology metrics

The uncertainty used in this study was defined as the 5th and 95th percentiles of the 100 Monte Carlo bootstrapping samples ranging from a few days to several weeks (**Table 2**). The uncertainty was the lowest for SOS and the highest for LOS; EOS had intermediate uncertainty. The highest uncertainty in LOS maybe because of the compounding effect of SOS and EOS (Yang and Noormets 2021). Generally, metrics

https://doi.org/10.5194/essd-2021-452
Preprint. Discussion started: 31 March 2022

of grasslands had the lowest uncertainty: SOS uncertainty ranged from 3.8 to 5.1 days, EOS uncertainty ranged from 8.6 to 10.4 days, LOS uncertainty ranged from 13.7 to 14.2 days; forests have the largest uncertainty, with SOS uncertainty ranging from 7.3 to 9.4 days, EOS uncertainty from 16.0 to 18.4 days, and LOS uncertainty from 25.4 to 25.7 days. The high uncertainty in the forests was possibly because this ecosystem included multiple mixed vegetation types and the phenology of these plants was more difficult to retrieve (Piao et al. 2019).

4.5 Changes in photosynthetic phenology metrics

We conducted the linear regression analysis by using the transition dates of phenology and the time series in each grid cell, and the regression coefficient was considered as the changing trend of the grid cell (**Fig. 6**). Here, we only showed the changes of the dominant single growing season. For the spatial distribution of the phenology metrics with the three thresholds, 61.71-64.25% of the study area experienced advanced trends of SOS, with a large advanced trend in northwestern North America, northern Siberia, and eastern Europe (changes>0.6 days $year^{-1}$); 57.97%-65.89% of the study area

https://doi.org/10.5194/essd-2021-452
Preprint. Discussion started: 31 March 2022

experienced delayed trends of EOS, with a large delayed trend in the northern North America and northern Siberia (changes>0.4 days year^{-1}); 70.29-70.76% of the study area experienced extended trends of LOS, with a large extended trend in northern China, northern North America, and northern Siberia (changes>0.6 days year^{-1}). Note that the inconsistent climate change trends in different seasons may lead to advanced or delayed SOS and EOS in some regions simultaneously, such as eastern Europe (Cohen et al. 2012).

We spatially averaged the phenology metrics for the terrestrial ecosystems across the Northern Hemisphere to assess the interannual variation of phenology metrics (**Fig. 7**). During the period 2001-2020, the mean SOS of all thresholds significantly advanced by 0.13-0.16 days year^{-1} (p<0.05); the mean EOS of 10% and 25% significantly advanced by 0.03-0.35 days year^{-1} (p<0.05); the mean LOS of all thresholds significantly extended by 0.16-0.51 days year^{-1} (p<0.01). These findings are consistent with previous studies (Zhu et al. 2012, Liu et al. 2016). For example, Liu et al. (2016) indicated that the EOS delayed by 0.18 days year^{-1} across the Northern Hemisphere of 1982-2011.

https://doi.org/10.5194/essd-2021-452
Preprint. Discussion started: 31 March 2022

5. Data availability

This dataset is divided into single and double growing seasons. The entire dataset is deposited at the open-access repository Figshare (https://doi.org/10.6084/m9.figshare.17195009.v2; Fang et al. 2021).

6. Conclusions

This study used a long-term (2001-2020) SIF-based GPP product (GOSIF-GPP) to generate annual photosynthetic phenology of vegetation with a high spatial resolution (0.05°) in the Northern Hemisphere. Here, we applied a method combining filter smoothing and change point detection to determine the annual dynamics of phenology metrics (i.e., SOS, EOS, and LOS). This method avoided the re-modeling of the GPP time series and allowed the extraction of metrics with different thresholds in multiple growing seasons. We provided data users with three choices (10%, 25%, and 50%

https://doi.org/10.5194/essd-2021-452
Preprint. Discussion started: 31 March 2022

threshold) of the metrics most appropriate for their specific application. Overall, the photosynthetic phenology metrics based on GOSIF-GPP agree with those extracted from in situ observations of EC towers. Compared to the metrics of vegetation indices and MODIS-GPP, the GOSIF-GPP metrics can provided more accurate phenology in most EC tower sites. The comparison with field data acquired at the EC towers suggests the 25% threshold of GOSIF-GPP can better capture the dynamics of photosynthetic phenology than other thresholds. In addition, the results showed a spatially explicit pattern from the north to the south in Northern Hemisphere. The SOS of all thresholds presented a significant advanced trend in the past 20 years; the EOS of 50% threshold showed an insignificant delayed trend; the LOS of all thresholds had a significant extended trend.

The phenology product based on GOSIF-GPP in our study is of great use in vegetation phenology studies because the SIF can directly reveal seasonal variations in vegetation vital activities (Mohammed et al. 2019). With these metrics, the response of vegetation phenology to climate change can be further investigated such as the importance of precipitation in spring phenology (Li et al. 2021). It will also be useful

https://doi.org/10.5194/essd-2021-452
Preprint. Discussion started: 31 March 2022

for developing and validating dynamic vegetation models. Our phenology metrics could be further improved when more accurate SIF-based GPP estimates are available.

Acknowledgments

This study was supported by the National Natural Science Foundation of China (32101349, 32171599). This study also was supported by the National Key R&D Program of China (2019YFA0606904) and the Key Program of the National Natural Science Foundation of China (32130069). J.X. was supported by the University of New Hampshire.

Reference

Badgley, G., Field, C. B., & Berry, J. A. 2017. Canopy near-infrared reflectance and terrestrial photosynthesis. Science Advances, **3**:e1602244.

Baldocchi, D., Falge, E., Gu, L., Olson, R., Hollinger, D., Running, S., ... & Wofsy, S. 2001. FLUXNET: A new tool to study the temporal and spatial variability of ecosystem-scale carbon dioxide, water vapor, and energy flux densities. Bulletin of the American Meteorological Society, **82**: 2415-2434.

Bertani, G., F. H. Wagner, L. O. Anderson, and L. E. O. C. Aragão. 2017. Chlorophyll Fluorescence Data

https://doi.org/10.5194/essd-2021-452
Preprint. Discussion started: 31 March 2022

Open Access Earth System Science Data Discussions

Reveals Climate-Related Photosynthesis Seasonality in Amazonian Forests. Remote Sensing **9**:1275.

Chen, A., J. Mao, D. Ricciuto, D. Lu, J. Xiao, X. Li, P. E. Thornton, and A. K. Knapp. 2021. Seasonal changes in GPP/SIF ratios and their climatic determinants across the Northern Hemisphere. Global Change Biology **27**:5186-5197.

Cohen, J. L., J. C. Furtado, M. Barlow, V. A. Alexeev, and J. E. Cherry. 2012. Asymmetric seasonal temperature trends. Geophysical Research Letters **39**.

Dai, J., M. Zhu, W. Mao, R. Liu, H. Wang, J. M. Alatalo, Z. Tao, and Q. Ge. 2021. Divergent changes of the elevational synchronicity in vegetation spring phenology in North China from 2001 to 2017 in connection with variations in chilling. International Journal of Climatology **41**:6109-6121.

Efron, B. 1992. Bootstrap Methods: Another Look at the Jackknife. Pages 569-593 *in* S. Kotz and N. L. Johnson, editors. Breakthroughs in Statistics: Methodology and Distribution. Springer New York, New York, NY.

Elmore, A. J., S. M. Guinn, B. J. Minsley, and A. D. Richardson. 2012. Landscape controls on the timing of spring, autumn, and growing season length in mid-Atlantic forests. Global Change Biology **18**:656-674.

Fang, J., J. A. Lutz, L. Wang, H. H. Shugart, and X. Yan. 2020. Using climate-driven leaf phenology and growth to improve predictions of gross primary productivity in North American forests. Global Change Biology **26**:6974-6988.

Fang, J., Li, X., X. Xiao, J., X. Yan, B. Li, F. Liu. 2021. Vegetation photosynthetic phenology metrics in northern terrestrial ecosystems: a dataset derived from a gross primary productivity product based on solar-induced chlorophyll fluorescence. figshare. Dataset. https://doi.org/10.6084/m9.figshare.17195009.v1

Frankenberg, C., C. O'Dell, J. Berry, L. Guanter, J. Joiner, P. Köhler, R. Pollock, and T. E. Taylor. 2014. Prospects for chlorophyll fluorescence remote sensing from the Orbiting Carbon Observatory-2. Remote Sensing of Environment **147**:1-12.

Garrity, S. R., G. Bohrer, K. D. Maurer, K. L. Mueller, C. S. Vogel, and P. S. Curtis. 2011. A comparison of multiple phenology data sources for estimating seasonal transitions in deciduous forest carbon exchange. Agricultural and Forest Meteorology **151**:1741-1752.

Gu, L., Post, W. M., Baldocchi, D. D., Black, T. A., Suyker, A. E., Verma, S. B., ... & Wofsy, S. C. 2009. Characterizing the seasonal dynamics of plant community photosynthesis across a range of vegetation types. In Phenology of ecosystem processes (pp. 35-58). Springer, New York, NY.

Huang, X., J. Xiao, and M. Ma. 2019. Evaluating the Performance of Satellite-Derived Vegetation Indices

https://doi.org/10.5194/essd-2021-452
Preprint. Discussion started: 31 March 2022

for Estimating Gross Primary Productivity Using FLUXNET Observations across the Globe. Remote Sensing **11**:1823.

Joiner, J., Y. Yoshida, A. P. Vasilkov, K. Schaefer, M. Jung, L. Guanter, Y. Zhang, S. Garrity, E. M. Middleton, K. F. Huemmrich, L. Gu, and L. Belelli Marchesini. 2014. The seasonal cycle of satellite chlorophyll fluorescence observations and its relationship to vegetation phenology and ecosystem atmosphere carbon exchange. Remote Sensing of Environment **152**:375-391.

Joiner, J., Y. Yoshida, A. P. Vasilkov, Y. Yoshida, L. A. Corp, and E. M. Middleton. 2011. First observations of global and seasonal terrestrial chlorophyll fluorescence from space. Biogeosciences **8**:637-651.

Keenan, T. F., A. D. Richardson, and K. Hufkens. 2020. On quantifying the apparent temperature sensitivity of plant phenology. New Phytologist **225**:1033-1040.

Killick, R., P. Fearnhead, and I. A. Eckley. 2012. Optimal detection of changepoints with a linear computational cost. Journal of the American Statistical Association **107**:1590-1598.

Klosterman, S. T., K. Hufkens, J. M. Gray, E. Melaas, O. Sonnentag, I. Lavine, L. Mitchell, R. Norman, M. A. Friedl, and A. D. Richardson. 2014. Evaluating remote sensing of deciduous forest phenology at multiple spatial scales using PhenoCam imagery. Biogeosciences **11**:4305-4320.

Köhler, P., Frankenberg, C., Magney, T. S., Guanter, L., Joiner, J., & Landgraf, J. 2018. Global retrievals of solar-induced chlorophyll fluorescence with TROPOMI: First results and intersensor comparison to OCO-2. Geophysical Research Letters, **45**: 10-456.

Li, X., Y. H. Fu, S. Chen, Xiao J., G. Yin, X. Li, X. Zhang, X. Geng, Z. Wu, X. Zhou, J. Tang, and F. Hao. 2021. Increasing importance of precipitation in spring phenology with decreasing latitudes in subtropical forest area in China. Agricultural and Forest Meteorology **304-305**:108427.

Li, X., Xiao, J., He, B., Altaf Arain, M., Beringer, J., Desai, A. R., ... & Varlagin, A. 2018. Solar-induced chlorophyll fluorescence is strongly correlated with terrestrial photosynthesis for a wide variety of biomes: First global analysis based on OCO-2 and flux tower observations. Global change biology, **24**: 3990-4008.

Li, X., and J. Xiao. 2019. A global, 0.05-degree product of solar-induced chlorophyll fluorescence derived from OCO-2, MODIS, and reanalysis data. Remote Sensing **11**: 517.

Li, X., and J. Xiao. 2020. Global climatic controls on interannual variability of ecosystem productivity: Similarities and differences inferred from solar-induced chlorophyll fluorescence and enhanced vegetation index. Agricultural and Forest Meteorology **288-289**:108018.

Li, X., Y. Zhou, L. Meng, G. R. Asrar, C. Lu, and Q. Wu. 2019. A dataset of 30 m annual vegetation phenology indicators (1985–2015) in urban areas of the conterminous United States. Earth

https://doi.org/10.5194/essd-2021-452
Preprint. Discussion started: 31 March 2022

System Science Data **11**:881-894.

Liu, Q., Y. H. Fu, Z. Zhu, Y. Liu, Z. Liu, M. Huang, I. A. Janssens, and S. Piao. 2016. Delayed autumn phenology in the Northern Hemisphere is related to change in both climate and spring phenology. Global Change Biology **22**:3702-3711.

Meroni, M., M. Rossini, L. Guanter, L. Alonso, U. Rascher, R. Colombo, and J. Moreno. 2009. Remote sensing of solar-induced chlorophyll fluorescence: Review of methods and applications. Remote Sensing of Environment **113**:2037-2051.

Mohammed, G. H., R. Colombo, E. M. Middleton, U. Rascher, C. van der Tol, L. Nedbal, Y. Goulas, O. Pérez-Priego, A. Damm, M. Meroni, J. Joiner, S. Cogliati, W. Verhoef, Z. Malenovský, J.-P. Gastellu-Etchegorry, J. R. Miller, L. Guanter, J. Moreno, I. Moya, J. A. Berry, C. Frankenberg, and P. J. Zarco-Tejada. 2019. Remote sensing of solar-induced chlorophyll fluorescence (SIF) in vegetation: 50 years of progress. Remote Sensing of Environment **231**:111177.

Pastorello, G., Trotta, C., Canfora, E., Chu, H., Christianson, D., Cheah, Y. W., ... & Law, B. 2020. The FLUXNET2015 dataset and the ONEFlux processing pipeline for eddy covariance data. Scientific data **7**:225.

Piao, S., Q. Liu, A. Chen, I. A. Janssens, Y. Fu, J. Dai, L. Liu, X. Lian, M. Shen, and X. Zhu. 2019. Plant phenology and global climate change: Current progresses and challenges. Global Change Biology **25**:1922-1940.

Richardson, A. D., R. S. Anderson, M. A. Arain, A. G. Barr, G. Bohrer, G. Chen, J. M. Chen, P. Ciais, K. J. Davis, A. R. Desai, M. C. Dietze, D. Dragoni, S. R. Garrity, C. M. Gough, R. Grant, D. Y. Hollinger, H. A. Margolis, H. McCaughey, M. Migliavacca, R. K. Monson, J. W. Munger, B. Poulter, B. M. Raczka, D. M. Ricciuto, A. K. Sahoo, K. Schaefer, H. Tian, R. Vargas, H. Verbeeck, J. Xiao, and Y. Xue. 2012. Terrestrial biosphere models need better representation of vegetation phenology: results from the North American Carbon Program Site Synthesis. Global Change Biology **18**:566-584.

Richardson, A. D., K. Hufkens, T. Milliman, D. M. Aubrecht, M. Chen, J. M. Gray, M. R. Johnston, T. F. Keenan, S. T. Klosterman, and M. Kosmala. 2018. Tracking vegetation phenology across diverse North American biomes using PhenoCam imagery. Scientific data **5**:1-24.

Richardson, A. D., T. F. Keenan, M. Migliavacca, Y. Ryu, O. Sonnentag, and M. Toomey. 2013. Climate change, phenology, and phenological control of vegetation feedbacks to the climate system. Agricultural and Forest Meteorology **169**:156-173.

Seyednasrollah, B., D. R. Bowling, R. Cheng, B. A. Logan, T. S. Magney, C. Frankenberg, J. C. Yang, A. M. Young, K. Hufkens, M. A. Arain, T. A. Black, P. D. Blanken, R. Bracho, R. Jassal, D. Y. Hollinger, B.

E. Law, Z. Nesic, and A. D. Richardson. 2021. Seasonal variation in the canopy color of temperate evergreen conifer forests. New Phytologist **229**:2586-2600.

Sjöström, M., M. Zhao, S. Archibald, A. Arneth, B. Cappelaere, U. Falk, A. de Grandcourt, N. Hanan, L. Kergoat, W. Kutsch, L. Merbold, E. Mougin, A. Nickless, Y. Nouvellon, R. J. Scholes, E. M. Veenendaal, and J. Ardö. 2013. Evaluation of MODIS gross primary productivity for Africa using eddy covariance data. Remote Sensing of Environment **131**:275-286.

Smith, W. K., J. A. Biederman, R. L. Scott, D. J. P. Moore, M. He, J. S. Kimball, D. Yan, A. Hudson, M. L. Barnes, N. MacBean, A. M. Fox, and M. E. Litvak. 2018. Chlorophyll Fluorescence Better Captures Seasonal and Interannual Gross Primary Productivity Dynamics Across Dryland Ecosystems of Southwestern North America. Geophysical Research Letters **45**:748-757.

Tang, J., Zeng, J., Zhang, Q., Zhang, R., Leng, S., Zeng, Y., ... & Wang, Q. 2020. Self-adapting extraction of cropland phenological transitions of rotation agroecosystems using dynamically fused NDVI images. International journal of biometeorology, 64: 1273-1283.

Verma, M., D. Schimel, B. Evans, C. Frankenberg, J. Beringer, D. T. Drewry, T. Magney, I. Marang, L. Hutley, C. Moore, and A. Eldering. 2017. Effect of environmental conditions on the relationship between solar-induced fluorescence and gross primary productivity at an OzFlux grassland site. Journal of Geophysical Research: Biogeosciences **122**:716-733.

Walther, S., Voigt, M., Thum, T., Gonsamo, A., Zhang, Y., Köhler, P., ... & Guanter, L. 2016. Satellite chlorophyll fluorescence measurements reveal large-scale decoupling of photosynthesis and greenness dynamics in boreal evergreen forests. Global change biology, **22**: 2979-2996.

Wang, X., Xiao, J., Li, X., Cheng, G., Ma, M., Che, T., ... & Wu, J. 2017. No consistent evidence for advancing or delaying trends in spring phenology on the Tibetan Plateau. Journal of Geophysical Research: Biogeosciences, **122**: 3288-3305.

Wang, X., Xiao, J., Li, X., Cheng, G., Ma, M., Zhu, G., Arain, M.A., Black, T.A., Jassal, R.S. 2019. No trends in spring and autumn phenology during the global warming hiatus. Nature communications **10**: 1-10.

Wood, J. D., T. J. Griffis, J. M. Baker, C. Frankenberg, M. Verma, and K. Yuen. 2017. Multiscale analyses of solar-induced florescence and gross primary production. Geophysical Research Letters **44**:533-541.

Wu, C., D. Peng, K. Soudani, L. Siebicke, C. M. Gough, M. A. Arain, G. Bohrer, P. M. Lafleur, M. Peichl, A. Gonsamo, S. Xu, B. Fang, and Q. Ge. 2017. Land surface phenology derived from normalized difference vegetation index (NDVI) at global FLUXNET sites. Agricultural and Forest Meteorology **233**:171-182.

https://doi.org/10.5194/essd-2021-452
Preprint. Discussion started: 31 March 2022

Open Access Earth System Science Data Discussions

Xiao, J., Chevallier, F., Gomez, C., Guanter, L., Hicke, J.A., Huete, A.R., Ichii, K., Ni, W., Pang, Y., Rahman, A.F., Sun, G., Yuan, W., Zhang, L., Zhang, X. 2019. Remote sensing of the terrestrial carbon cycle: A review of advances over 50 years. Remote Sensing of Environment, 233:111383.

Yang, L., and A. Noormets. 2021. Standardized flux seasonality metrics: a companion dataset for FLUXNET annual product. Earth System Science Data **13**:1461-1475.

Zhao, M., Heinsch, F. A., Nemani, R. R., & Running, S. W. 2005. Improvements of the MODIS terrestrial gross and net primary production global data set. Remote Sensing of Environment, **95**:164-176.

Zhao, R.-F., X.-P. Chen, F.-S. Zhang, H. Zhang, J. Schroder, and V. Römheld. 2006. Fertilization and Nitrogen Balance in a Wheat–Maize Rotation System in North China. Agronomy Journal **98**:938-945.

Zhu, W., Tian, H., Xu, X., Pan, Y., Chen, G., & Lin, W. 2012. Extension of the growing season due to delayed autumn over mid and high latitudes in North America during 1982–2006. Global Ecology and Biogeography, **21**: 260-271.

Table 1. Statistical comparison of the phenology metrics retrieved from EC tower GPP and GOSIF-GPP, NDVI, EVI, NIRv, and MODIS-GPP. 10%, 25%, and 50% mean the three thresholds. The bold means the highest *R* and the lowest *RMSE*. *R*: correlation coefficient; *RMSE*: root mean square error.

Data source	SOS			EOS			LOS		
	10%	25%	50%	10%	25%	50%	10%	25%	50%
	R								
GOSIF-GPP	**0.79**	**0.80**	**0.78**	**0.63**	**0.73**	0.63	**0.72**	**0.76**	**0.65**
NDVI	0.14	0.25	0.39	0.45	0.42	0.56	0.28	0.32	0.40
EVI	0.40	0.46	0.57	0.57	0.60	0.66	0.37	0.37	0.38
NIRv	0.47	0.51	0.60	**0.63**	0.66	**0.67**	0.51	0.48	0.41
MODIS-GPP	0.66	0.67	0.65	0.29	0.55	0.61	0.47	0.55	0.49
***RMSE* (days)**									
GOSIF-GPP	**18.03**	**15.83**	**14.99**	**23.55**	**21.89**	24.38	**33.93**	**29.14**	**27.89**

https://doi.org/10.5194/essd-2021-452
Preprint. Discussion started: 31 March 2022

NDVI	36.91	32.18	26.20	34.13	39.68	41.86	53.87	53.92	52.39
EVI	36.97	31.34	24.97	31.75	29.41	26.09	58.53	49.04	39.28
NIRv	29.86	26.00	21.74	27.26	25.67	24.95	46.11	40.03	35.12
MODIS-GPP	22.98	20.56	18.83	30.22	24.76	**23.88**	43.79	36.33	32.25

Table 2. The mean value and uncertainty of photosynthetic phenology metrics in the different terrestrial ecosystems.

Terrestrial ecosystems	**Threshold**	**Mean SOS (uncertainty)**	**Mean EOS (uncertainty)**	**Mean LOS (uncertainty)**
Forests	10%	108.26 (7.34)	271.29 (18.39)	163.03 (25.73)
	25%	122.12 (8.28)	255.40 (17.31)	133.28 (25.59)
	50%	138.44 (9.38)	236.24 (16.01)	97.80 (25.40)
Shrublands	10%	75.10 (5.09)	144.33 (9.78)	69.22 (14.88)
	25%	80.97 (5.49)	137.14 (9.30)	56.17 (14.79)
	50%	88.14 (5.97)	129.02 (8.75)	40.89 (14.72)
Savannas	10%	106.37 (7.21)	244.25 (16.56)	137.88 (23.77)
	25%	117.25 (7.95)	230.10 (15.60)	112.85 (23.55)
	50%	130.85 (8.87)	213.10 (14.45)	82.24 (23.32)
Grasslands	10%	56.72 (3.84)	153.48 (10.40)	96.76 (14.25)
	25%	65.21 (4.42)	140.37 (9.52)	75.16 (13.94)
	50%	74.71 (5.06)	127.55 (8.65)	52.84 (13.71)
Wetlands	10%	106.58 (7.23)	213.13 (14.45)	106.55 (21.67)
	25%	115.24 (7.81)	202.70 (13.70)	86.83 (21.51)
	50%	126.24 (8.56)	189.61 (12.85)	63.37 (21.41)
Croplands	10%	86.60 (5.87)	272.47 (18.47)	185.87 (24.34)
	25%	102.20 (6.93)	250.78 (17.00)	148.58 (23.93)
	50%	120.56 (8.17)	226.01 (15.32)	105.45 (23.49)

https://doi.org/10.5194/essd-2021-452
Preprint. Discussion started: 31 March 2022

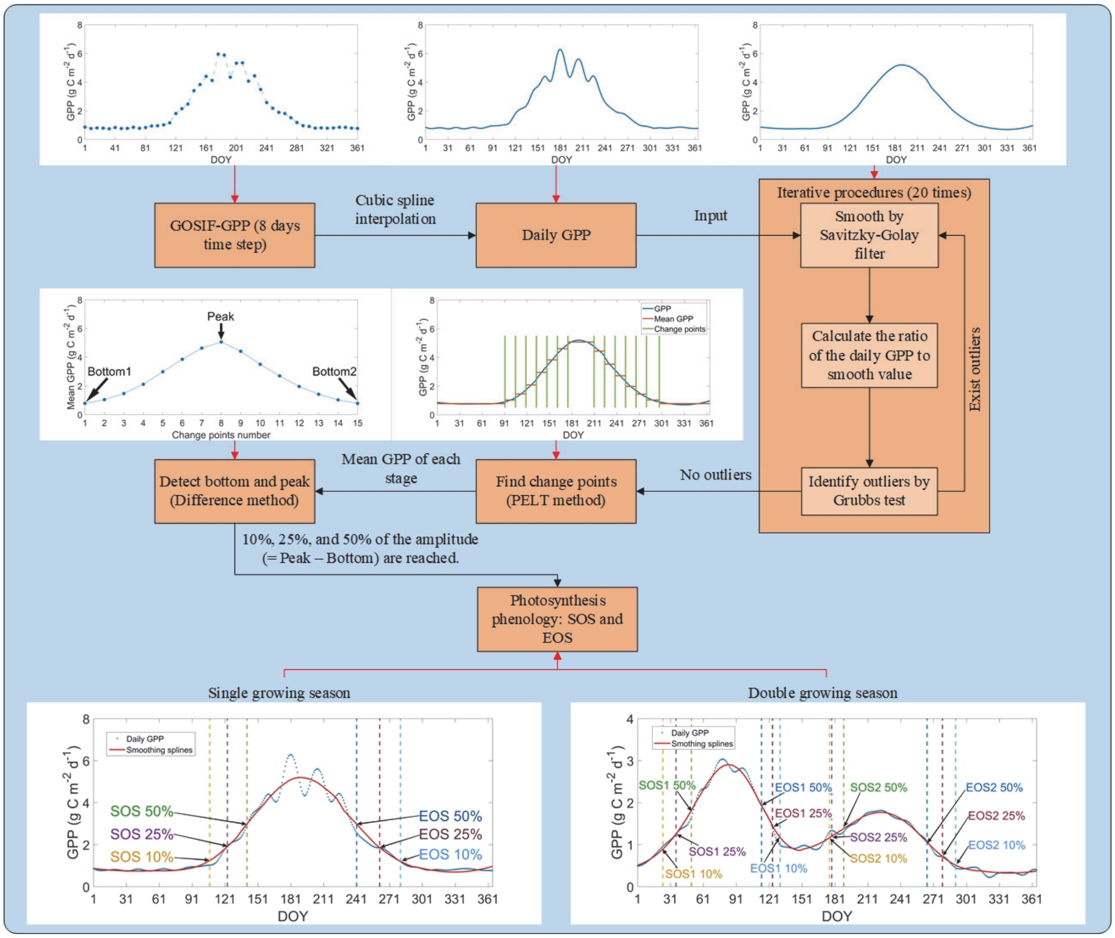

Fig. 1. Illustration of the method for identifying the transition dates of photosynthetic phenology. The method is based on three thresholds, 10%, 25%, and 50%. Bottom1: baseline for dormancy season before the growing season; Peak: the peak value in one single cycle; Bottom2: baseline for dormancy season after growing season. The example of the single growing season is from one forest site (latitude: 60.0° N, longitude: 15.5° E); the example of the double growing season is from one cropland site (latitude: 36.5° N, longitude: 36.0° E).

https://doi.org/10.5194/essd-2021-452
Preprint. Discussion started: 31 March 2022

Earth System Science Data
Open Access Discussions

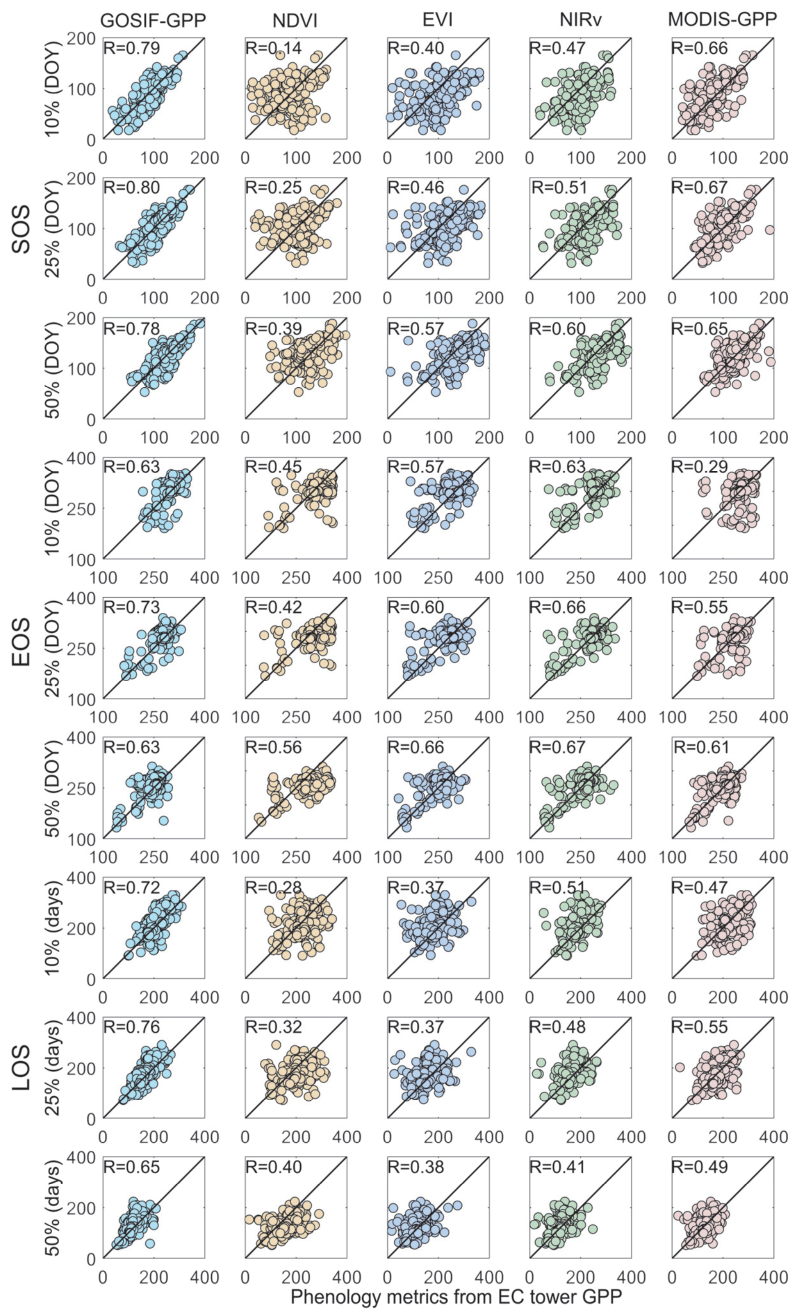

Fig. 2. The comparison of the phenology metrics retrieves from EC tower GPP and GOSIF-GPP, NDVI, EVI, NIRv, and MODIS-GPP. The dotted line represents a 1:1 line. DOY: day of the year; R: correlation coefficient.

https://doi.org/10.5194/essd-2021-452
Preprint. Discussion started: 31 March 2022

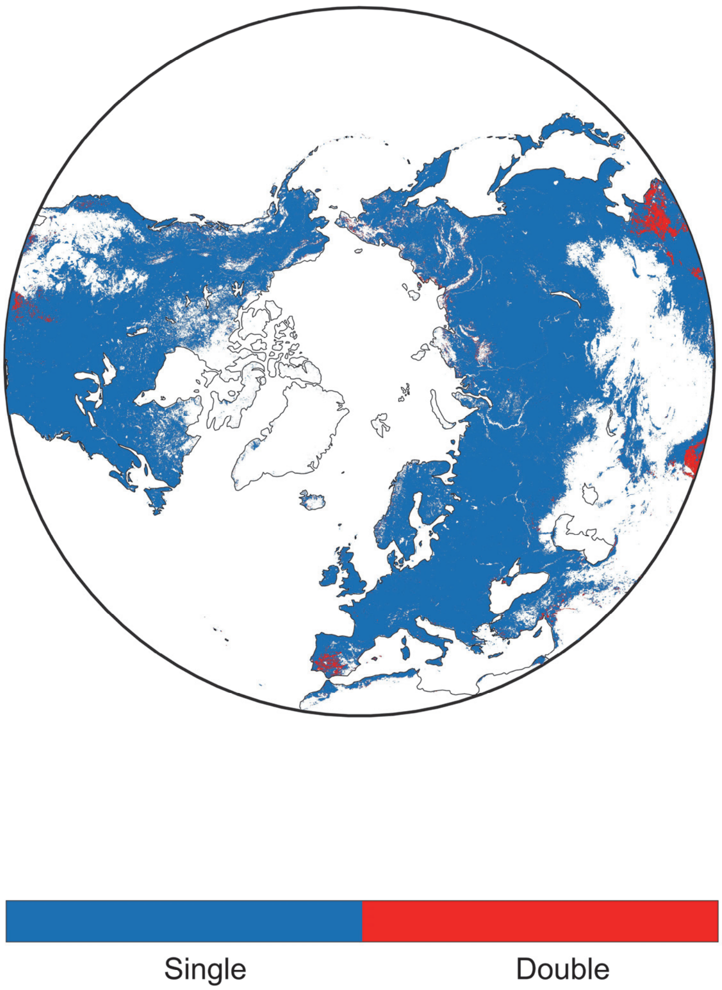

Fig. 3. The spatial distribution of the number of growing seasons in the Northern Hemisphere (0.05° spatial resolution).

https://doi.org/10.5194/essd-2021-452
Preprint. Discussion started: 31 March 2022

Open Access Earth System Science Data Discussions

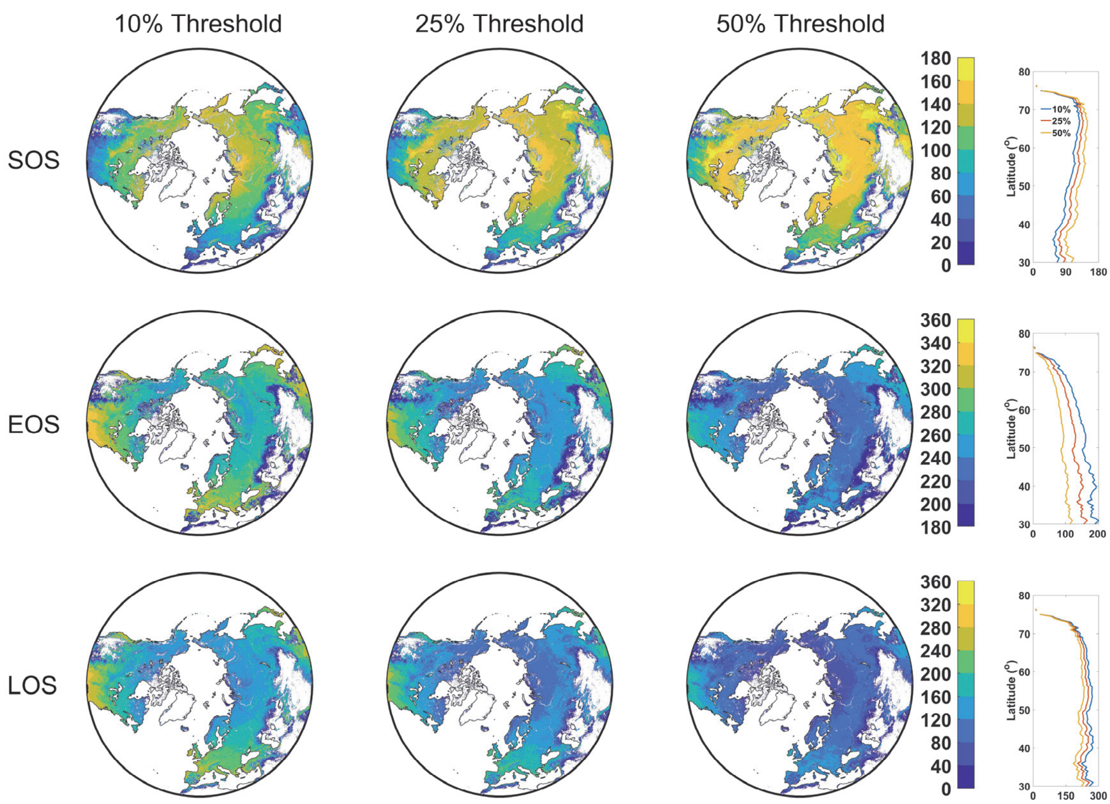

Fig. 4. The spatial distribution of the mean photosynthetic phenology metrics (first growing season) in the Northern Hemisphere of 2001-2020 (0.05° spatial resolution). The right parts are the latitudinal pattern.

https://doi.org/10.5194/essd-2021-452
Preprint. Discussion started: 31 March 2022

Open Access Earth System Science Data Discussions

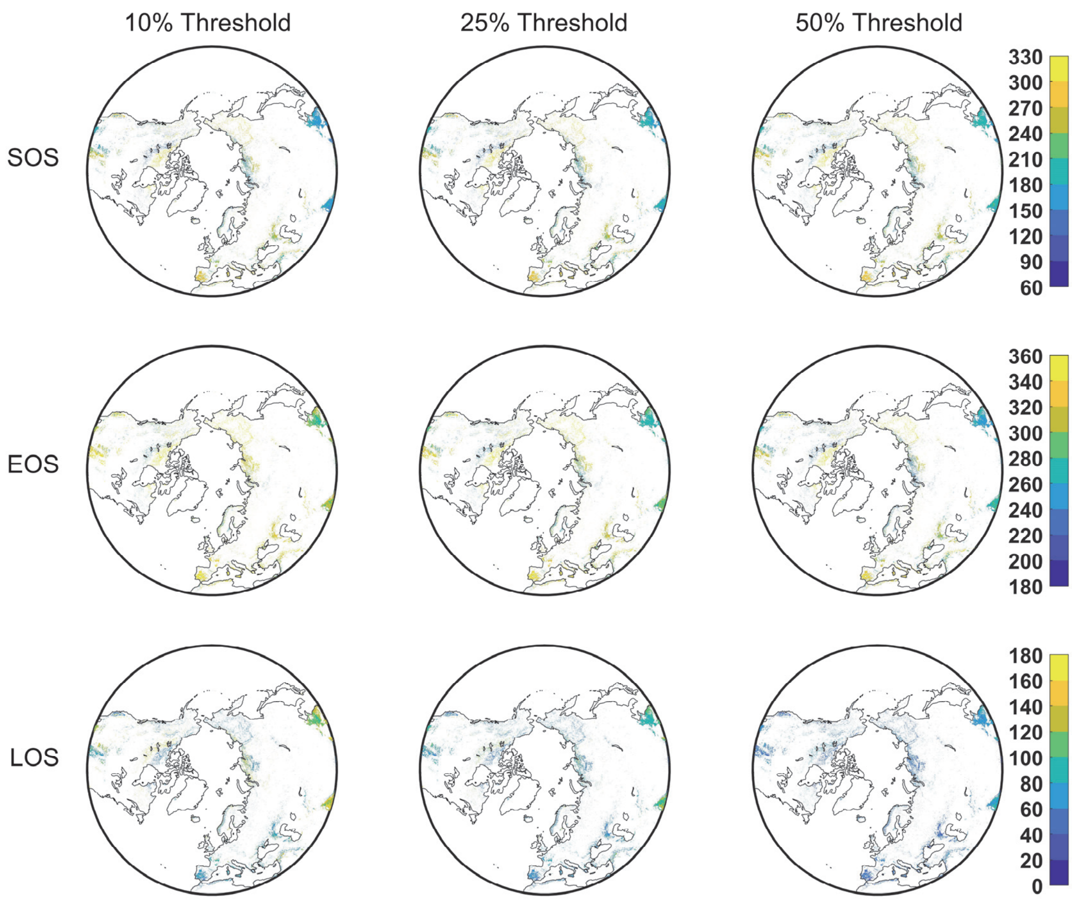

Fig. 5. The spatial distribution of the mean photosynthetic phenology metrics of the second growing season in the Northern Hemisphere of 2001-2020 (0.05° spatial resolution).

https://doi.org/10.5194/essd-2021-452
Preprint. Discussion started: 31 March 2022

Open Access Earth System Science Data Discussions

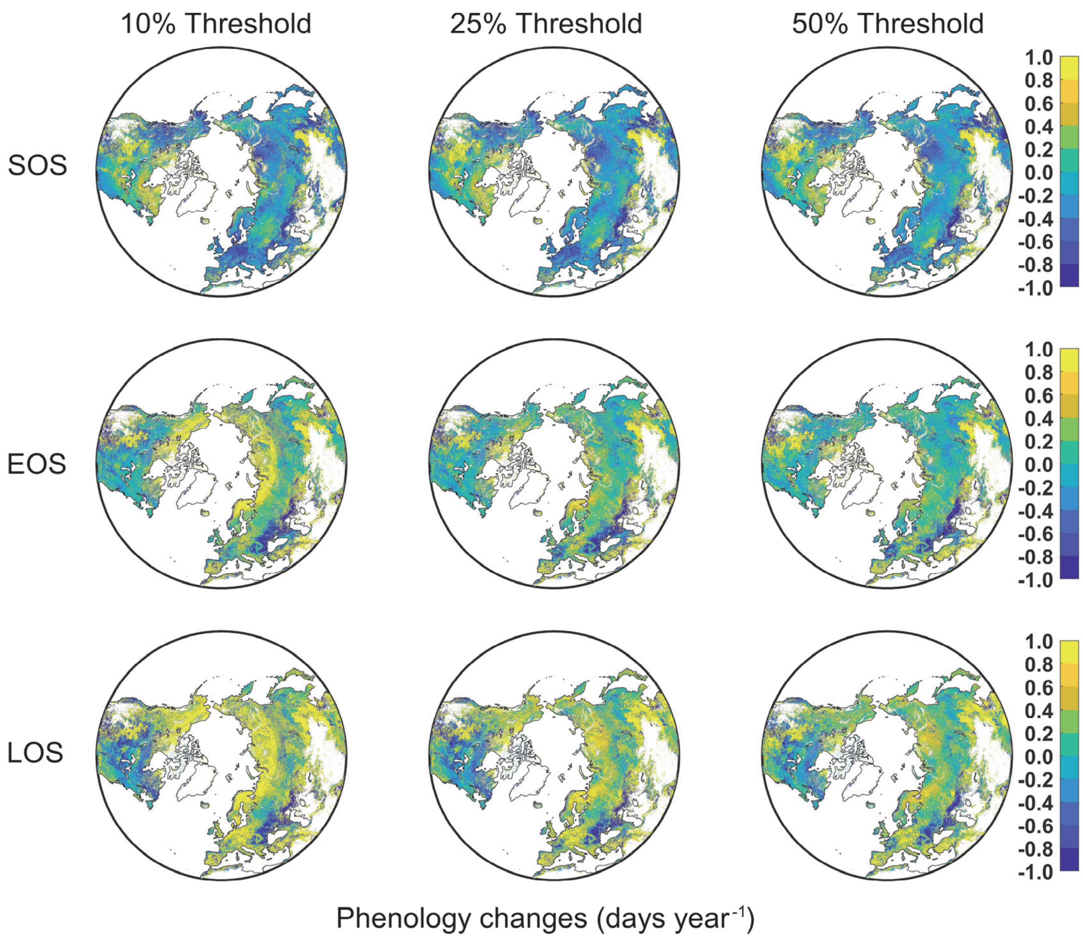

Fig. 6. Changes in photosynthetic phenology metrics in the Northern Hemisphere over the period 2001-2020.

https://doi.org/10.5194/essd-2021-452
Preprint. Discussion started: 31 March 2022

Open Access Earth System Science Data Discussions

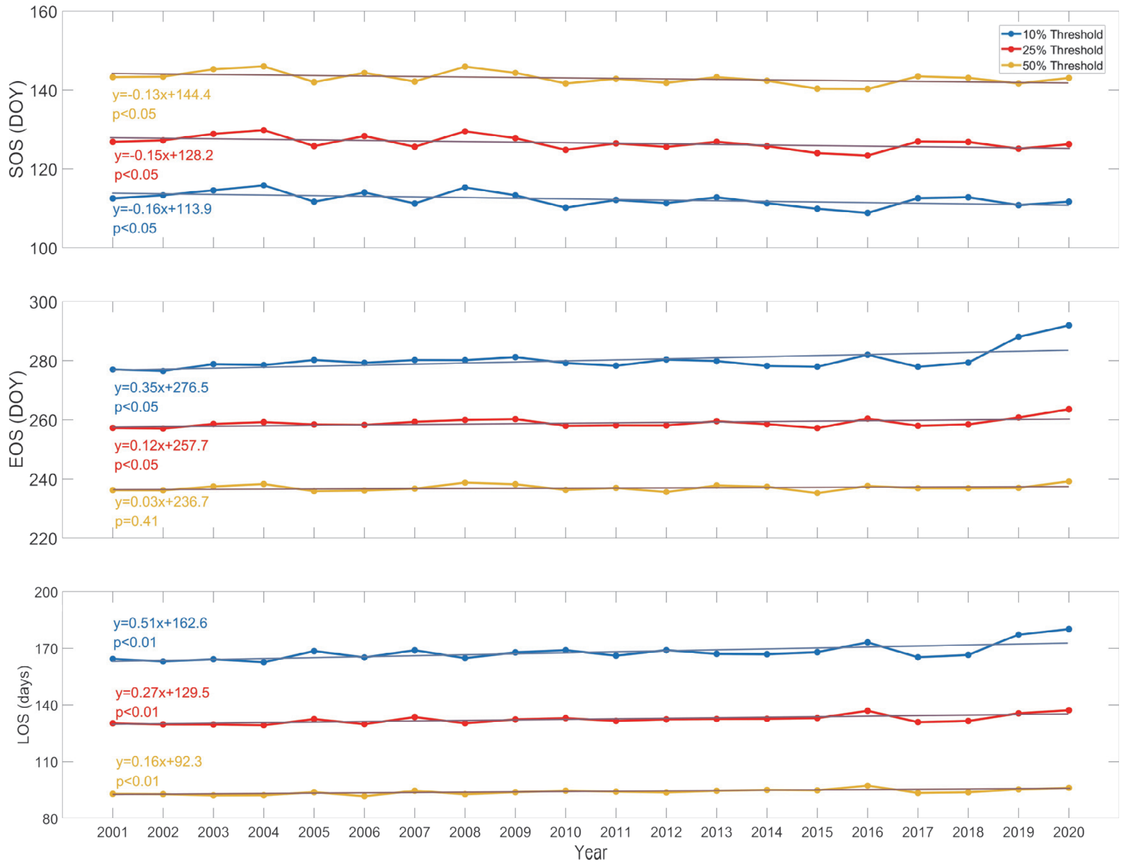

Fig. 7. Annual photosynthetic phenology metrics in the Northern Hemisphere during 2001-2020. The straight lines represent the change trends.